Journal of Alloys and Compounds xxx (xxxx) 170067

Contents lists available at ScienceDirect

Journal of Alloys and Compounds

journal homepage: www.elsevier.com/locate/jallcom

Cluster variation method for investigation of multi-principal-element metallic alloys

Rémy Besson

Univ. Lille, CNRS, INRAE, Centrale Lille, UMR 8207 - UMET - Unité Matériaux et Transformations, F-59000 Lille, France

ARTICLE INFO

Article history:
Received 23 January 2023
Received in revised form 27 March 2023
Accepted 8 April 2023

Keywords:
Multi-principal-element alloys
Phase diagrams
Cluster variation method
Phase. separation
Long-range ordering

ABSTRACT

We present atomic-scale investigations of the thermodynamic properties of quinary bcc-based multi-principal-element alloys (MPEAs) within {Al,Co,Cr,Fe,Mn,Mo,Ni}, by means of short-range pair energetics and the cluster variation method (CVM) in the irregular tetrahedron approximation. We focus on an essential couple of key-properties detrimental for potential applications of MPEAs, namely the trends to (i) long-range ordering (LRO) and (ii) phase separation (PS). While the CVM has been more commonly employed in a grand canonical frame controlled by chemical potentials (δμ), we propose an original δμ-driven CVM scheme which allows an easier exploration of wide composition spaces typical of MPEAs. This modified scheme yields a slice-by-slice analysis of this space, by means of pseudo-ternary isothermal sections, which demonstrates the ability of the CVM to lead, with moderate computational effort, to full phase diagrams of MPEAs. In particular, our CVM calculations provide elements to interpret recent unexpected experimental trends of AlCrFeMnMo. Comparison with earlier studies of the same MPEAs using the less accurate point-mean-field (PMF) approximation indicates that CVM and PMF have global agreement for LRO at higher temperatures, whereas CVM should definitely be preferred as soon as PS begins to occur. Both approaches, employed more systematically in future MPEA studies in conjunction with ab initio electron theory and dedicated experiments, may offer convenient tools to check the merits of, and even improve, the various sets of effective pair interactions nowadays increasingly available for atomic-scale simulations of MPEAs, thus helping to identify composition domains relevant to avoid trends (i) and (ii) and design more reliable MPEAs.

1. Introduction

Multi-principal-element alloys (MPEAs), a huge class of metallic alloys encompassing "chemically complex alloys" (CCAs) or "high-entropy alloys" (HEAs), have been regarded as promising materials for roughly two decades [1,2]. In contrast with conventional alloys, built upon a single base element and several minor additions, MPEAs are characterized by a higher number - at least three, but often five or beyond - of principal elements in roughly equal proportions, frequently leading to simple bcc or fcc crystallographic structures. Whereas the composition space of MPEAs is extremely large, making its exploration difficult, it is a widely-known fact that MPEAs with tuned compositions may offer outstanding properties. In particular, mechanical properties of MPEAs are usually assumed to be related to the more or less random mixing, thus with no long-range ordering, of the various metallic species on the lattice sites. Due to the strong resulting lattice distortions, this atomic-scale multi-element mixing, typical of MPEAs, should be responsible for the hindering of the motion of dislocations, thus leading to enhanced mechanical properties.

Even though possibilities of reinforcement of MPEAs by dispersed additional ordered phases are now increasingly regarded, reference cases for MPEAs do still consist of single-phase disordered solid solutions. It is therefore relevant to get a deeper knowledge of the physical factors controlling the emergence and stability of the random mixing of metallic species in the solid solution usually constituting the main part of MPEA-based systems. This phenomenon is frequently referred to as MPEA stabilization by high configuration entropy, hence the HEA acronym. To this purpose, it is essential to investigate in detail MPEA thermodynamics [3], since the latter field is the most valuable guide, providing important information for MPEA design, in particular as regards the composition ranges for which single-phase disordered solid solutions should be achievable. In this respect, two main trends are worth exploring with particular attention, i.e. those trends related to (i) long-range ordering (LRO) and (ii) phase separation (PS). A deeper knowledge of this couple of key-trends should help to get a quick overview of the merits of various candidate MPEA systems.

To carry out such thermodynamic explorations, phenomenological CALPHAD-type calculations are highly valuable tools, since they offer the advantage of encompassing wide composition spaces, together with

https://doi.org/10.1016/j.jallcom.2023.170067
0925-8388/© 20XX

the formation and stability of all kinds of (meta)stable phases, irrespective of their crystal structures. For MPEA studies, the latter feature constitutes a key-advantage, because such systems, though primarily built on a unique bcc or fcc underlying lattice, are often observed to contain various other non-cubic, sometimes unexpected and undesired additional phases, usually intricate ordered compounds such as intermetallics or carbides [4]. In this context, CALPHAD approaches offer a convenient way to propose various scenarios of thermal treatments that may help monitor, either promote or hinder, the formation of these additional phases, leading to the possibility of multiphase MPEAs with controlled properties. However, the success of this task strongly depends on the thermodynamic databases employed, an issue which may turn out to be critical in practice. More precisely, in contrast with more conventional alloys, e.g. steels or aluminium alloys, for which reliable specialized thermodynamic databases have been built, similar databases for MPEAs often remain sparse, which allows some room for alternative approaches, in particular those relying on atomic-scale formulations of thermodynamics.

To explore the thermodynamic trends of MPEAs from the atomic scale, it is common to take advantage from the simple cubic crystal structure of these systems, which allows building various configuration energy models from the powerful cluster expansion approach [5,6]. Using such flexible energy models, Monte-Carlo (MC) algorithms then offer a straightforward atomic-scale thermodynamic framework to simulate heat treatments and monitor the phase stability of MPEAs [7]. However, in order for atomic-scale thermodynamic simulations to be reliable, the most critical issue is related to the achievement of the configuration energy models that should be employed for MPEAs, since the multi-element nature of these systems may drastically increase the intricacy of such models. In the current state of research, the elaboration of configuration energies for MPEAs mostly relies on ab initio electron methods [8], in particular density functional theory, and two main paths can be followed. The first path, resting on high-throughput procedures, consists in exploiting the correlation between the available structures and energies taken from wide ab initio databases of ordered compounds, in order to infer effective interactions between chemical species. These interactions are then supposed to be transferable to the bcc or fcc atomic environments of MPEAs. A key-feature related to transferability concerns the fact that these interactions are assumed to be composition-independent. Following this path led to propose [9] first-nearest-neighbour pair energy coefficients for a large panel (~30) of elements, which allowed subsequent applications to several practically appealing quinary MPEA alloys, namely within A-B-C-D-E systems with {A,B,C,D,E} belonging to {Al,Co,Cr,Fe,Mn,Mo,Ni}, including the effect of slight composition changes around the reference equiatomic alloys $A_{0.2}B_{0.2}C_{0.2}D_{0.2}E_{0.2}$ [10,11]. In spite of these advantages, the physical insight into the effective interactions obtained from this first path remains limited. As a consequence, a second path may also be followed, which is intrinsically designed to overcome this deficiency. This second path relies on the disordered nature of MPEAs, which allows building effective interactions from a theoretical description of the disordered alloy, taken as a reference medium, and described via the coherent potential approximation (CPA). This second path produces composition-dependent effective interactions, and allows proposing elements of interpretation for the magnitude and sign of these interactions. It was applied recently [12] to investigate phase stability in equiatomic CoCrFeMnNi MPEAs.

Reliable atomistic energy models, although a cornerstone, are not the only issue for atomic-scale thermodynamics of MPEAs. As already mentioned, composition spaces of MPEAs are immense and difficult to explore, and faced with this difficulty, and even assuming a reliable energetics at hand, the thermodynamic treatment itself is also at stake. In many practical cases, MPEA elaboration involves steps of initial composition guesses, possibly followed by subsequent composition readjustments aimed at improving some target properties. Since such strategic reorientations, during the course of elaboration processes, may be exceedingly costful in terms of experimental efforts, it is desirable that atomic-scale thermodynamics be able to investigate and predict the effects of virtual composition changes, especially on the aforementioned key-trends (i) and (ii), in order to help select those composition shifts which may best be worth carrying out experimentally. In this respect, MC simulations, while mostly accurate, remain computationally expensive, and thus can be performed only for restricted families of candidate MPEAs with well-chosen compositions. This emphasizes the relevance of complementary atomic-scale thermodynamic tools allowing investigations of more extended composition domains of MPEAs. To this purpose, we proposed previously [13] a handsome point-mean-field (PMF) approach, designed to yield pseudo-ternary isothermal sections of phase diagrams for quinary MPEAs. Using an alloy energetics described by effective first-nearest-neighbour (1N) pair interactions, the application of PMF thermodynamics to the case of quinary AlCrFeMnMo with bcc structure, a system of practical interest recently investigated from experiments [14], allowed to demonstrate the tractability of this approach and estimate its degree of accuracy, by comparison with exact MC simulations for the same alloy energetics. As shown in this earlier work, a noticeable interest of PMF thermodynamics concerns its ability to provide a quick survey of the trends of an MPEA system to LRO and PS around its reference equiatomic composition. However, it is a general fact [12] that PMF approaches usually tend to overestimate LRO, and a similar limitation can be pointed out [15] for PS, which in PMF tends to be overdelayed at cooling. An appealing way to overcome these difficulties consists in resorting to the cluster variation method (CVM) [5,16], which can be viewed as an improved version of PMF, keeping good tractability due to its analytic formulation and easy numerical resolution. More specifically, the CVM in the tetrahedron approximation, used extensively for binary systems and more scarcely for ternary ones [17,18], should also be well suited for MPEAs [19,20], since these alloys often have bcc or fcc cubic structures. The CVM should therefore be used to investigate with success, primarily the qualitative key-trends (i) and (ii) of MPEAs, but also more quantitative estimations of critical LRO and PS temperatures, as well as finer features of LRO or short-range ordering (species-dependent site occupancies, pair correlation functions…).

In this context, the major task of the present work will be to provide a thorough analysis of the merits of the CVM approach to MPEA thermodynamics for predictions of trends (i) and (ii), including wide composition domains as well as comparisons with earlier MC and PMF results on the same alloys. However, extending the CVM to perform investigations of wide MPEA composition spaces is not as obvious as expected, since this approach is usually formulated in a (semi-)grand canonical way (GC-CVM) controlled by chemical potentials, whereas it is more desirable to handle composition constraints. More precisely, by definition of MPEAs, studies of these systems are mainly concerned with their behaviour around the central part of the composition space (equiatomic alloy), whereas it is quite useless to explore other domains, in particular those domains closer to the corners of the phase diagram. Besides, we intend to make extensive use of pseudo-ternary isothermal sections, since the relevance of this representation for MPEAs was shown previously [13]. Therefore, in order to match these requirements, a proper adaptation of the GC-CVM method will be relevant, and prior to any presentation of MPEA trends, this issue will thus form a preliminary topic of the present work.

The present CVM study will be mostly dedicated to MPEAs from the AlCrFeMnMo system, because earlier atomic-scale thermodynamic investigations of this system from MC [11] and PMF [13] simulations are available, and this quinary system was recently shown to be potentially useful for coating applications [14]. Moreover, in accordance with earlier works [10,11,13], two other quinary systems will be also investigated, namely AlCoCrFeNi and AlCrFeMnNi, allowing (i) to draw comparisons between alloys from the AlCoCrFeNi → AlCrFeMnNi → AlCr-

FeMnMo sequence, a situation corresponding to gradual element-by-element substitutions and thus typical of alloy selection, (ii) to enhance the reliability of our conclusions on the respective merits of CVM, MC and PMF for MPEAs. Therefore, the present CVM study will be carried out using the same ab initio-based 1N pair alloy energetics [9] already employed in the aforementioned earlier works [10,11,13] on these systems. This is only a matter of convenience for our purpose of comparison, and as also pointed out for PMF [13], the CVM approach presented below could also be straightforwardly generalized in presence of 2 N pair interactions.

To summarize, the present work is thus devoted to a thorough application of the CVM approach in the irregular tetrahedron approximation to several neighbouring bcc-based quinary MPEAs. We make use of an ab initio-based 1N pair energetics available in the literature [9], while the CVM approach is also suited to include 2 N pairs. We focus on bcc alloys, being primarily concerned with the ill-known AlCrFeMnMo system studied recently [14], but we also include in our analysis the neighbouring AlCoCrFeNi and AlCrFeMnNi systems, in order to encompass the AlCoCrFeNi → AlCrFeMnNi → AlCrFeMnMo sequence of alloy selection. To investigate the strengths and weaknesses of CVM for MPEAs, we also make appropriate comparisons with a couple of previous works [11,13] concerned respectively with the same alloys using MC and PMF simulations.

2. Methods

Our intention here is to describe a procedure designed to perform CVM thermodynamics on MPEAs. Before this, it is worth justifying our choice to keep, for these investigations, the most standard framework of CVM, which relies on its GC formulation. Indeed, in analogy with our previous work devoted to PMF thermodynamics of MPEAs [13], it might seem quite natural to try using a "constrained CVM" formalism, allowing to carry out a slice-by-slice building of the phase diagram by means of pseudo-ternary isothermal sections. By selecting only composition points belonging to the selected section, this constrained approach would entail a significant reduction of the computational cost, i.e. an appealing feature for quinary MPEAs which may even become mandatory if higher-order systems were to be explored in future. By contrast, the common GC-CVM approach, even after some optimization (see below) to limit the range of chemical potentials considered, inherently remains more cumbersome, because it requires some exploration of composition domains, either not useful, since located outside the isothermal section of interest, or redundant if several sections are built in sequence for different values of the constraints. In principle, taking into account constraints on the atomic fractions (x_D et x_E for quinary A-B-C-D-E), which proved successful in PMF [13], should be possible in CVM too, since the self-consistent procedure of resolution of the main equations, yielding the site or cluster occupancies, are similar in PMF and CVM respectively. However, the formal complexity of the thermodynamic approach being higher in CVM than in PMF, the handling of the auxiliary treatment required to solve for x_D and x_E should be trickier in CVM than in PMF. In addition, our previous work [13] suggested that, in analogy with PMF, a "constrained CVM" formulation may also be unexpectedly uneasy to handle in practice, especially at lower temperatures prone to phase separations. More precisely, the practical application of "constrained PMF" was found to experience difficulties related to convergence failures if the composition constraints fall within a phase separation domain. This implied [13] the requirement to be able to detect, when PMF convergence cannot be reached, whether this convergence failure is due to some numerical artifact (e.g. choice of initial values of occupation variables), or if this is the signature of some genuine phase separation. For all these reasons, we have preferred leaving for later works these interesting but complex issues of formulating and applying "constrained CVM" to MPEAs, and we have thus preserved in this work the standard GC-CVM formalism recalled briefly now.

The CVM, especially in the so-called "tetrahedron approximation" useful for cubic systems, is a well-documented atomic-scale method for alloy thermodynamics [5,16–18]. We thus now outline briefly its main features, with focus on the grand-canonical (GC) formulation of the CVM in the irregular tetrahedron approximation [17,18], for an A-B-C-D-E quinary substitutional bcc alloy. For substitutional bcc alloys, the CVM formalism relies on the usual decomposition of the crystal into four sublattices $S \in \{\alpha,\beta,\gamma,\delta\}$ - by convention, we choose α and β on cube corners, while γ and δ are on cube centers. For bcc crystals, the irregular tetrahedron corresponds to the maximal cluster taken into account in the CVM approximate expression of the probability density yielding the entropy of the system. In this "maximal cluster probability" formulation, the resolution of the CVM equations in the tetrahedron approximation is frequently performed through a so-called "natural iteration method" (NIM), which is an efficient self-consistent fixed-point algorithm, the convergence of which usually requires a small number of iterations. Since this resolution is carried out for each set of elemental chemical potentials, building phase diagrams of quinary MPEAs thus requires to perform a four-fold scan in {B,C,D,E} chemical potentials, the quantities scanned being $\delta\mu^r = \mu^r - \mu^A$ for r ∈{B,C,D,E}, A being the "background element" (A = Fe in our work, this choice being immaterial). In the irregular tetrahedron approximation, the CVM configurational energy, involving 1N and 2 N pairs, is written in terms of the corresponding energy coefficients also present in the PMF formalism for quinary MPEAs described previously [13], namely for each neighbor shell (q = 1 or 2), the 10-element set $\left\{J_{qN}^{BB}, J_{qN}^{BC}, J_{qN}^{BD}, J_{qN}^{BE}, J_{qN}^{CC}, J_{qN}^{CD}, J_{qN}^{CE}, J_{qN}^{DD}, J_{qN}^{DE}, J_{qN}^{EE}\right\}$. In the CVM formalism, it is convenient to express the average alloy energy $\langle E\rangle$as a function of the probability system $\{w_{ijkl}\}$ of a tetrahedron (maximal cluster), which is the set of CVM unknowns to be determined by the NIM procedure:

$$\langle E\rangle = 6N \sum_{i,j,k,l} w_{ijkl}\varepsilon_{ijkl}$$

(i,j,k,l) labelling respectively the chemical species on the {α,β,γ,δ} sublattices. In the CVM study of MPEAs reported below, the alloy energetics is restricted to q = 1, these 1N pair coefficients {J} being deduced from the ab initio energy data $\{H^{ij}\}$ provided in an earlier work [9], using the correspondence between the {H} and {J} data given in our previous PMF study [13]. In this context restricted to 1N pairs, the connection between the {J} and {ε} coefficients takes the expression provided in the appendix.

Having briefly described the CVM approach in the tetrahedron approximation, it is worth recalling here that this methodology was extensively applied, a few decades ago, to a quite large number of bcc-based binary (meta)stable systems, and more scarcely to several cases of ternary ones. While for binary cases this easily led to entire (meta)stable phase diagrams, studies of ternary systems were restricted to more partial isothermal sections. As mentioned above, the latter convenient representation, which should probably be privileged for higher-order systems, was thus maintained, by means of additional constraints, in our earlier PMF study of quinary MPEAs [13]. In this context, before tackling our main topic of interest devoted to quinary MPEAs, it is instructive to present briefly GC-CVM for a quaternary system handled by a full three-dimensional scan of chemical potentials. To this aim, we consider the case of bcc AlCrFeMn described by a generic configuration energy including both 1N and 2 N pairs. This energy model was built by extension from an earlier modeling [15] of ternary AlFeMn designed, in the context of steels, to reproduce more specifically the Fe corner of the phase diagram. Being thus probably not reliable to capture the behaviour of AlCrFeMn around the equiatomic domain, it was not employed further in our study of quinary MPEAs, and will merely serve here for purpose of illustration in a quaternary case. Using this generic "toy model", the bcc-based isothermal phase diagram of AlCrFeMn at 1000 K is plotted (Fig. 1) by means of the usual three-dimensional tetrahedron representation of composition space. As already mentioned in

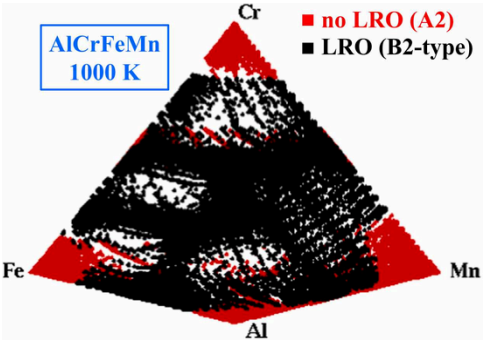

Fig. 1. Calculated phase diagram (CVM in irregular tetrahedron approximation) of quaternary bcc AlCrFeMn at 1000 K, showing A2 and B2-type domains in black and red respectively. The underlying energy model, a generic one used for purpose of illustration only, differs from the 1N pair model employed throughout below for the various quinary systems explored.

earlier works [11,13], in view of our purpose of exploring the main trends to LRO and PS of MPEAs, and faced with the exceedingly wide variety of LROs possibly occurring in high-order systems, we decided to restrict our analysis by discriminating MPEAs through a simpler "LRO vs no LRO" criterion. This choice was also motivated by the fact that the 1N pair energetics, used previously and below for quinary MPEAs within {Al,Co,Cr,Fe,Mn,Mo,Ni}, significantly reduces this complexity, since it allows only the A2 bcc solid solution (absence of LRO) or B2-type LRO, thus discarding more intricate situations such as B32, $D0_3$, $L2_1$ and XA compounds. For this preliminary study of AlCrFeMn, although a much richer panel of LROs would be allowed by the presence of 2N interactions in the generic model, we thus employed the same simplified criterion, and the red and black colours on Fig. 1 denote respectively the A2 and B2-type regions of composition space. Fig. 1 provides an overview of the trends to LRO of this model quaternary AlCrFeMn, indicating, as expected, the presence of the A2 solid solution near each corner, while LRO appears to occur quite soon when getting away from these corners. However, it is obviously difficult to infer the behaviour in the concentrated MPEA domain, in which the trends to LRO or PS are hidden, and a more thorough analysis thus requires iso-composition cuts. This was performed at nearly-constant x_{Cr} (Fig. 2a), by means of a narrow composition filter x_{Cr} ~5 % selecting only those points with $0.04 < x_{Cr} < 0.06$ - similar composition filters on x_D et x_E will be employed for quinary MPEAs, see next section. For comparison, Fig. 2b displays the behaviour obtained from x_{Cr}-constrained PMF. It demonstrates a good qualitative agreement between CVM and PMF as regards the respective locations of A2 and B2-type LROs. As expected from usual features of PMF approaches, the agreement is however lower for PS trends, with the opening of a PS domain near the Al corner predicted by CVM, whereas this domain is absent in PMF. For a given energy model, assuming CVM to be a reasonably accurate thermodynamic approach (this issue will examined in detail for quinary MPEAs

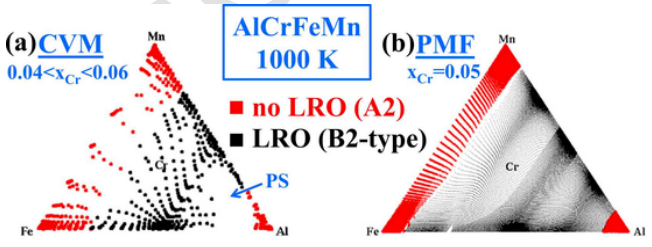

Fig. 2. Pseudo-ternary section (AlFeMn plane) of the calculated isothermal AlCrFeMn phase diagram at 1000 K (Fig. 1), under the constraint of (nearly) constant $x_{Cr} = 5$ %: (a) CVM (constraint imposed approximately via a composition filtering), (b) PMF (exact constraint). As in Fig. 1, the underlying energy model is a generic one.

in the next section), as opposed to more approximate PMF, this CVM vs PMF comparison of model AlCrFeMn confirms that PMF may be used as an efficient preliminary tool for sketching a panorama of LRO trends of an MPEA. A similar analysis (not shown for brevity) was carried out for x_{Cr} ~25 %, namely in a composition domain more typical of MPEAs, confirming the same qualitative agreement between CVM and PMF on LRO and underestimation of PS trends in PMF.

As mentioned previously, the most straightforward extension of this GC-CVM approach to quinary MPEAs requires a four-fold scan of chemical potentials, using a hypercubic four-dimensional domain $\{\delta\mu_i\}$ with similar ranges along the four directions. A raw application of this 4D scan would be however too cumbersome and useless, since only the center region of the phase diagram is concerned by MPEAs. Instead, it is more relevant to employ a procedure similar to that described previously for PMF [13], namely to resort to pseudo-ternary isothermal sections in the ABC plane, encompassing the target equiatomic alloy, and complying with two composition constraints, usually $x_D = x_E = 1/5$. Prior to the main CVM calculations, the overall procedure involves thus a preliminary step, the purpose of which is to determine a rectangular-shaped domain for $\{\delta\mu_i\}$ optimized for investigations of the selected x_D- and x_E-constrained composition areas, namely discarding as much as possible the manifold of useless dilute alloys located near the corners of the composition space and likely to be explored with a "hypercubic" scan. Moreover, as recalled in the introduction, an extensive characterization of MPEAs belonging to a quinary system A-B-C-D-E can efficiently be achieved by exploring the various pseudo-ternary isothermal sections in the ABC plane, for selected atomic fractions x_D and x_E. The main focus being on MPEAs which are concentrated alloys, it is therefore natural to start from the center of any section, i.e. from a point P with composition $x_P = x_A = x_B = x_C = [1 - x_D - x_E]/3$, and focus the exploration on a limited area with triangular shape circumventing P and homothetic to the triangle of the pseudo-ternary section. The dimension (position of corners) of this triangular area can then be settled through a parameter α in such a way that, for the close-to-A corner, $x_A = x_P + \alpha$ and $x_B = x_C = [1 - x_A - x_D - x_E]/2$, the other two corners of this triangular domain being then obtained similarly by circular permutations of the roles of A, B and C. For given values of α, x_D and x_E, the optimized rectangular domain for $\{\delta\mu_i\}$ related to this α-dependent composition range is then obtained using a modified "$\delta\mu$-driven" version of the CVM, designed to approach each corner (A, B and C in turn) of the pseudo-ternary isothermal section. To this aim, the GC-CVM was encapsulated into a gradient-like external algorithm, which allows to drive the chemical potentials toward each limiting composition point on the pseudo-ternary section. As explained just above, these limiting points are defined from a choice of α implying, for the largest ranges of explorations considered, $x_B = x_C = 2$ % for both species B and C opposite to the corner A of the isothermal section, namely $\alpha = 36$ % for $x_D = x_E = 20$ % sections, and $\alpha = 43.3$ % for the additional case $x_{Cr} = 22$ %, $x_{Mo} = 7$ % considered below. The convergence of this $\delta\mu$-driven CVM algorithm is illustrated on Fig. 3 for the Fe-corner of equiatomic AlCrFeMnMo (with an element labelling defined as A = Fe, B = Al, C = Mn, D = Cr, E = Mo), showing that a small number of steps is required for the chemical potential drag, in order to reach the target composition, $x_{Fe} = 56$ %, $x_{Al} = x_{Mn} = 2$ %, $x_{Cr} = x_{Mo} = 20$ % on the figure. Noticeably, this approach, computationally much cheaper than "raw hypercubic" scans, offers the advantage of being transposable to higher-order systems, thus improving GC-CVM tractability for such heavier systems. In practice, the preliminary determination of the optimized $\{\delta\mu_i\}$ domain was carried out at a single, relatively high temperature (1500 K for all alloys below), which ensures that (i) the composition domain explored is sufficiently large at all temperatures, since for a given $\{\delta\mu_i\}$ domain this area becomes wider when the temperature decreases, and that (ii) no phase-separation can cripple the determination of the $\{\delta\mu_i\}$ domain (the $\delta\mu$-driven CVM may fail to converge if it crosses unexpected phase-separated regions).

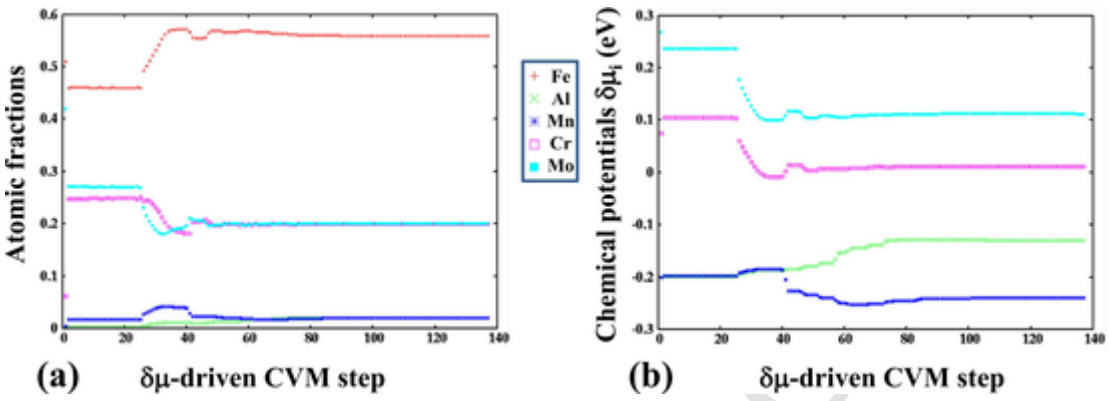

Fig. 3. In, the case of AlCrFeMnMo, profiles of (a) atomic fractions and (b) chemical potentials during the δμ-driven CVM algorithm used in the preliminary phase carried out to optimize the chemical potential scan, in order to encompass an adjustable composition domain for the selected composition constraints. The case considered here corresponds to the Fe-rich corner of the pseudo-ternary AlFeMn section and constraints $x_{Cr} = x_{Mo} = 20$ %. Convergence is usually reached in a small number of steps.

Table 1 displays the optimized $\{\delta\mu_i\}$ domains obtained for the four alloys studied. It shows that, as a rule of thumb, the optimization procedure allows significant shrinking of the required $\{\delta\mu_i\}$ ranges along both directions corresponding to the constrained elements (though this feature is less visible for Mo). Also remarkably (see element-dependent colors in Table 1), the required range - more visibly its lower bound - for a given element (e.g. Al or Cr) depends (i) on the system in which it is immersed, (ii) on the composition constraints selected within the same system, here AlCrFeMnMo. For the main CVM explorations described in the next section, these $\{\delta\mu_i\}$ domains were eventually employed in the whole temperature range investigated for each alloy. To this aim, they were subdivided into 4D regular grids with spacing $\Delta(\delta\mu) = 10$ meV, this value being reduced to 5 meV for lower temperatures, in order to better characterize PS trends.

Before considering nearly full ($\alpha = 0.36$) pseudo-ternary isothermal sections, it is instructive to conclude this part by describing succinctly (Fig. 4) the application of the δμ-driven CVM scheme to a more restricted ($\alpha = 0.16$) exploration of AlCrFeMnMo, using the selected ab initio-based 1N pair energetics [9], around the center P of the $x_{Cr} = x_{Mo} \sim 20$ % section. As shown on Fig. 4, apart from the missing area due to PS along the Fe-Mn axis, the expected triangular shape of the domain explored is reached only approximately, due to the non-linear relation between chemical potentials and composition. This is however not critical, and demonstrates that such a restricted and computationally cheap investigation should be sufficient to provide locally trends (i) and (ii), corresponding to various composition shifts, around the equiatomic alloy $Al_{0.2}Cr_{0.2}Fe_{0.2}Mn_{0.2}Mo_{0.2}$ (green dot on Fig. 4) usually taken as reference for MPEAs. Interestingly, taking into account that the A2 → B2-type transition of $Al_{0.2}Cr_{0.2}Fe_{0.2}Mn_{0.2}Mo_{0.2}$ occurs at 1200 K (figure not shown for brevity), comparison of Fig. 4a and b shows that a relatively narrow temperature range ~ 200 K is sufficient for this alloy to undergo successively LRO and PS, a feature that could be checked easily by dedicated experiments.

3. Results

This section is intended to describe the application of CVM simulations to explore the thermodynamic properties of selected MPEAs, with particular emphasis on predicting the influence of composition shifts on trends to LRO and PS. This task is the complement and generalization of previous studies [11,13] carried out on the same alloys by closely related atomic-scale methods, namely PMF and MC. In order to allow careful inspection of the respective merits of these methods, we will thus follow the same overall scheme as in these earlier studies, by considering MPEA systems obtained from the $AlCoCrFeNi \xrightarrow{Co \longrightarrow Mn} AlCrFeMnNi \xrightarrow{Ni \longrightarrow Mo} AlCrFeMnMo$ sequence of chemical substitutions. As explained in the previous section, we will build, for decreasing temperatures, pseudo-ternary isothermal sections at approximately fixed atomic fractions x_D and x_E for a couple of chemical species chosen for convenience, namely (Cr;Ni), (Mn;Ni) and (Cr;Mo) for the three aforementioned quinary systems, respectively. While inspecting the merits of CVM for MPEA thermodynamics, comparison with accurate MC simulations is not exhaustive [11], because the latter approach is restricted to few selected compositions and hardly allows building phase diagrams. Therefore, earlier MC results will be recalled and used as reference only for LRO and PS critical temperatures. Conversely, comparison between CVM and PMF is straightforward for critical temperatures and phase diagrams, and will thus be done systematically below. To this aim, the reader is referred to the PMF isothermal sections provided previously [13] and not reproduced here for brevity.

Table 1
Optimized $\{\delta\mu_i\}$ domains (eV) of chemical potentials relevant for pseudo-ternary sections of the four quinary alloys studied, and obtained using the δμ-driven CVM algorithm, for composition ranges corresponding to $\alpha = 0.36$ in the first three cases and $\alpha = 0.433$ in the last one – see text. While each alloy is labelled (top line) using alphabetic order for elements, the chemical potentials (second line) are labelled in B-C-D-E order, element A (= Fe chosen in all cases) omitted in the $\{\delta\mu_i\}$ line being the reference element used to define $\{\delta\mu_i\}$, and the composition constraints being relative to D and E. Element-dependent colors are also used to illustrate the sensitivity of each $\delta\mu_i$ range to systems and compositions. For the AlCrFeMnMo system, two alloy compositions are considered, either the reference equiatomic one, or a heuristically "optimized" [14] experimental alloy $Al_{22}Cr_{22}Fe_{29}Mn_{20}Mo_7$.

AlCoCrFeNi	AlCrFeMnNi	AlCrFeMnMo (equiat.)	$Al_{22}Cr_{22}Fe_{29}Mn_{20}Mo_7$ (opt.)
$\delta\mu_{Al} \times \delta\mu_{Co} \times \delta\mu_{Cr} \times \delta\mu_{Ni}$	$\delta\mu_{Al} \times \delta\mu_{Cr} \times \delta\mu_{Mn} \times \delta\mu_{Ni}$	$\delta\mu_{Al} \times \delta\mu_{Mn} \times \delta\mu_{Cr} \times \delta\mu_{Mo}$	$\delta\mu_{Al} \times \delta\mu_{Mn} \times \delta\mu_{Cr} \times \delta\mu_{Mo}$
[-0,430 ; 0,903]	[-0,448 ; 0,891]	[-0,130;0,906]	[-0,348 ; 1,065]
× [-0,391 ; 0,536]	× [-0,434 ; 0,438]	× [-0,240;0,352]	× [-0,455 ; 0,448]
× [-0,109 ; 0,497]	× [-0,143 ; 0,366]	× [0,011;0,455]	× [-0,104 ; 0,520]
× [-0,083 ; 0,424]	× [-0,105 ; 0,368]	× [0,112;0,904]	× [-0,119 ; 0,822]

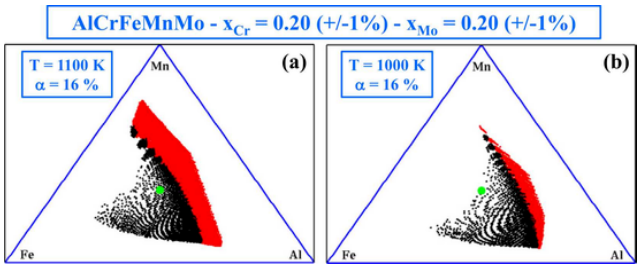

Fig. 4. Calculated phase diagram of AlCrFeMnMo (CVM in irregular tetrahedron approximation): pseudo-ternary section at 1000 K (approximate constraints $x_{Cr} = x_{Mo} = 20$ %), illustrating the application of the procedure to explore a limited domain (α = 16 % - see text for details) around the equiatomic alloy (green dot). The use of a finite, though small, window for x_{Cr} and x_{Mo} filtering induces a slight superposition effect visible on the figure, which however is immaterial for the identification of trends (i) and (ii).

3.1. AlCoCrFeNi

In our CVM investigations of MPEAs, we first consider the AlCoCrFeNi system, which has already formed the subject of recent studies [10,11,13], including comparisons between experiments and MC simulations with the 1N pair energetics employed in the present work. Fig. 5 displays the pseudo-ternary isothermal sections (AlCoFe plane) for $x_{Cr} = x_{Ni} = 20$ % and decreasing temperatures between 1600 and 800 K. The increment Δ(δμ) for chemical potential scan and the thickness ε for composition filtering were chosen respectively equal to 10 meV and 2 % for temperatures above 1300 K, while for better accuracy Δ(δμ) = 5 meV and ε = 2 % were preferred at lower temperatures. In AlCoCrFeNi, the emergence of B2-type LRO (black area) at cooling is found to propagate from the Al corner of the isothermal section, whereas the A2 disordered solid solution (red area) persists along the Fe-Co edge down to lower temperatures (800 K). For the equiatomic alloy (green spot on Fig. 5), the onset temperature for LRO predicted by CVM is 1500 K, while for similar high temperatures, the opening of a primary PS domain is also clearly visible along the Fe-Al axis. Along the isothermal section considered, the overall structure of the phase diagram - proportions of A2 disordered, B2-type LRO and PS domains - is roughly stable in a significant temperature range between 1300 K and 1000 K, while the primary PS domain suddenly spreads up to the equiatomic central zone as the temperature falls below 900 K.

The main trends for equiatomic AlCoCrFeNi are collected in Table 2, which displays the LRO and PS transition temperatures, derived either from the current CVM predictions or from earlier PMF and MC studies. The agreement between CVM and MC for T_{LRO} is good, which suggests that the CVM can safely be used to infer the A2 → B2-type transition behaviour of bcc MPEAs in wide composition domains. This agreement contrasts with the PMF approach, which induces a strong (~300 K) overestimation of T_{LRO}. As regards PS, Table 2 indicates that the agreement between MC and CVM is less obvious than for LRO, since T_{PS} from CVM is found to lie slightly above the PS temperature range determined directly from MC simulations, whereas T_{PS} from PMF lies beneath the MC temperature range. Whether this moderate PS discrepancy between CVM and MC is due to CVM overestimation of T_{PS} or to non-physical delay in MC simulations remains an open issue at this stage.

Further insight into the respective merits of the CVM, PMF and MC approaches can be gained by considering more precisely the kind of

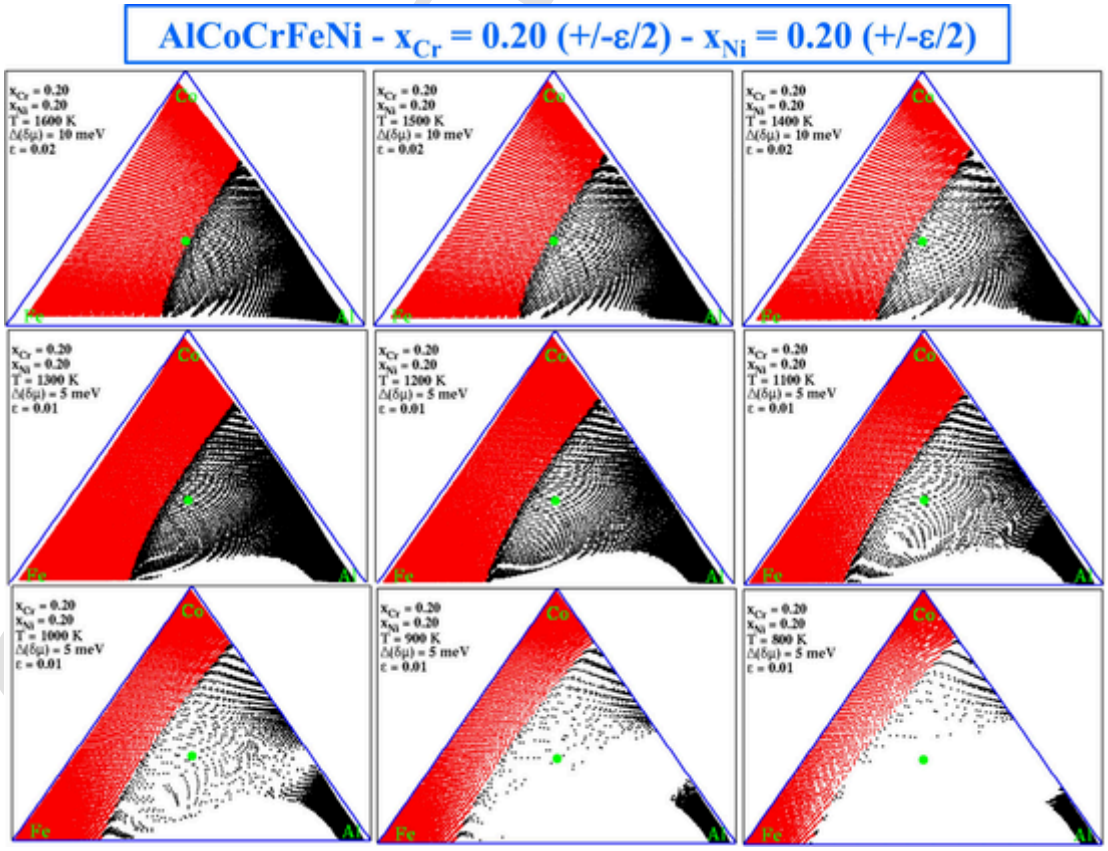

Fig. 5. Calculated phase diagram (CVM in irregular tetrahedron approximation) of bcc AlCoCrFeNi: isothermal pseudo-ternary sections in the AlCoFe plane for $x_{Cr} = x_{Ni} = 1/5$ (including the equiatomic alloy $Al_{0.2}Co_{0.2}Cr_{0.2}Fe_{0.2}Ni_{0.2}$, green spot) and decreasing temperatures, showing the trends to (i) LRO and (ii) PS for this model system described by ab initio-based 1N pair energetics. The disordered (A2) and ordered (B2-type) domains are displayed in red and black respectively. The simulation parameters ε and Δ(δμ) (respectively half-width of window for composition selection and step of the grid for chemical potential scan) are specified for each temperature (smaller ε and Δ(δμ) values are more suitable at lower temperatures).

Table 2
Transition temperatures (K) of trends to (i) long-range ordering (LRO) and (ii) phase separation (PS) for the MPEA quinary systems along the AlCoCrFeNi → AlCrFeMnNi → AlCrFeMnMo alloy sequence, from CVM thermodynamics (present work), as well as comparisons with previous estimations (between parentheses) of the same quantities, either from PMF calculations [13] or from direct MC simulations (Refs. [10] for AlCoCrFeNi and [11] for other alloys). For the AlCrFeMnMo system, two alloy compositions are considered, either the reference equiatomic one, or a heuristically "optimized" alloy $Al_{22}Cr_{22}Fe_{29}Mn_{20}Mo_7$ studied in earlier experiments [14]. Due to uncertainties inherent to direct MC simulations [11], the MC values of T_{PS} could only be localized within a temperature range. The last column provides the CVM species-dependent sublattice occupancies for the single-phase B2-type compound occurring below T_{LRO} in each system, together (between parentheses) with PMF and MC predictions recalled from the same earlier works [10,11,13]. Depending on the system, temperatures in the range 1000–1100 K (i.e. prior to PS occurrence) were selected for this sublattice analysis. It may be recalled that, in the A2 disordered state ($T > T_{LRO}$), the occupancies of each given species are sublattice-independent and all equal to its atomic fraction. In the PMF and MC compound formulae [13], only those species preferentially occupying a given sublattice are specified, {} symbols indicating secondary species, i.e. for which minor but non negligible sublattice occupancies were found. For unambiguous comparison between CVM, PMF and MC, it should be noted that the αβ and γδ sublattices play identical roles by symmetry, and can thus be exchanged.

	Trend (i) T_{LRO}	Trend (ii) T_{PS}	B2-type compound (for $T < T_{LRO}$)
AlCoCrFeNi (equiat.)	1500 (PMF: 2000) (MC: 1600)	900 (PMF: 500) (MC: 700–300)	$[Al_{38}Co_9Cr_{25}Fe_{21}Ni_7]_{\alpha\beta}[Al_2Co_{31}Cr_{15}Fe_{19}Ni_{33}]_{\gamma\delta}$ (PMF: $[CoFeNi]_{\alpha\beta}[AlCr\{Fe\}]_{\gamma\delta}$) (MC: $[CoNi]_{\alpha\beta}[AlCrFe]_{\gamma\delta}$)
AlCrFeMnNi (equiat.)	1300 (PMF: 1600) (MC: 1200)	1050 (PMF: 500) (MC: 900–300)	$[Al_{33}Cr_{21}Fe_{17}Mn_{19}Ni_{10}]_{\alpha\beta}[Al_7Cr_{19}Fe_{23}Mn_{20}Ni_{31}]_{\gamma\delta}$ (PMF: $[\{Cr\}FeMnNi]_{\alpha\beta}[AlCr\{Mn\}]_{\gamma\delta}$) (MC: $[CrFeMnNi]_{\alpha\beta}[AlCrFeMn]_{\gamma\delta}$)
AlCrFeMnMo (equiat.)	1200 (PMF: 1300) (MC: 1100)	1000 (PMF: < 300) (MC: 900–300)	$[Al_{26}Cr_{20}Fe_{10}Mn_{16}Mo_{28}]_{\alpha\beta}[Al_{14}Cr_{20}Fe_{30}Mn_{24}Mo_{12}]_{\gamma\delta}$ (PMF: $[AlCrMo]_{\alpha\beta}[\{Cr\}FeMn]_{\gamma\delta}$) (MC: $[AlCrMo]_{\alpha\beta}[CrFeMn]_{\gamma\delta}$)
$Al_{22}Cr_{22}Fe_{29}Mn_{20}Mo_7$ (optim.)	1050 (PMF: 1300) (MC: 1000)	850 (PMF: < 300) (MC: 700–300)	$[Al_{34}Cr_{24}Fe_{15}Mn_{15}Mo_{12}]_{\alpha\beta}[Al_9Cr_{20}Fe_{43}Mn_{25}Mo_3]_{\gamma\delta}$ (PMF: $[AlCrMo]_{\alpha\beta}[\{Cr\}FeMn]_{\gamma\delta}$) (MC: $[AlCrMo]_{\alpha\beta}[FeMn]_{\gamma\delta}$)

LRO which emerges in the B2-type equiatomic compound below T_{LRO} (Table 2). In equiatomic AlCoCrFeNi, the α and β sublattices, located on the same cube, are found to be occupied mainly by Al, then to a lesser extent by Cr and Fe, and finally by minor amounts of Co and Ni, while the γ and δ sublattices, located on the other cube, having a complementary behaviour, are mainly occupied by Co and Ni, to a lesser extent by Cr and Fe, and negligibly by Al. This can be written shortly, in decreasing order of occupancies, as $[Al > (Cr,Fe) > (Co,Ni)]_{\alpha\beta}$ $[(Co,Ni) > (Cr,Fe) > Al]_{\gamma\delta}$. Moreover, Fe and Cr display nearly random (~20 %, i.e. the overall atomic fraction of each species) distributions on the sublattices, which leads to the formula $[Al\{CrFe\}]_{\alpha\beta}[CoNi\{CrFe\}]_{\gamma\delta}$. Comparing this formula to its PMF and MC counterparts provided in Table 2 shows that, despite possible minor discrepancies on the sublattice attributions of Cr and Fe with quasi random behaviours, the agreement between the three approaches is satisfactory as regards sublattice occupancies in LRO states.

To conclude this part on AlCoCrFeNi, it is instructive to compare the above thermodynamic trends to the underlying energy parameters $\{H^{ij}\}$ already reported previously [13], and which can be classified as $H^{AlCo} \approx H^{AlNi} < H^{AlFe} < H^{AlCr} < H^{FeNi} < H^{CoFe} < H^{CrNi} < H^{CoNi} < H^{CrFe} < 0 < H^{CoCr}$. The main trend visible on the formulae of Table 2, namely the sharp sublattice partitioning between Al on the one hand and (Co,Ni) on the other hand, stems from the doublet of dominant attractive interactions $H^{AlCo} \approx H^{AlNi} < < 0$. It can also be noticed that the most negative values correspond to those parameters involving Al and any of the other four elements. Conversely, the nearly random behaviour of Cr and Fe is more difficult to infer from the set of $\{H^{ij}\}$. Therefore, even in the present context of very simple alloy energetics limited to 1N pairs, inspection of the $\{H^{ij}\}$ set is clearly not sufficient to infer LRO and PS properties of MPEAs, and to this purpose, thermodynamic simulations are thus mandatory.

3.1.1. AlCrFeMnNi

Following our guidelines, we now consider the predicted thermodynamic properties of MPEAs in the AlCrFeMnNi system, deduced from AlCoCrFeNi by substituting Co with Mn. As concerns the current 1N pair alloy energetics (H^{ij} from Table 1 of Ref. [13]), this corresponds to replace the Co-X interactions by Mn-X ones, namely to the replacement of the strongly attractive Al-Co interaction by the more moderate attractive Al-Mn one, while other interactions relevant to the Co → Mn substitution remain roughly unaltered. Fig. 6 displays isothermal pseudo-ternary sections (AlCrFe plane, constraints $x_{Mn} = x_{Ni} = 1/5$) of the AlCrFeMnNi phase diagram for decreasing temperatures between 1600 and 800 K. As regards LRO trends, we note an early propagation of B2-type ordering from the Al corner, whereas a significant composition domain along the Cr-Fe axis remains disordered down to moderate temperatures. In this respect, when comparing AlCoFe and AlCrFe pseudo-ternary sections, the overall behaviour of AlCrFeMnNi is quite similar to that described previously for AlCoCrFeNi (Fig. 5). The similarity between both systems is less marked for PS trends, since PS in AlCrFeMnNi is found to develop simultaneously near the Al-Fe and Al-Cr axes, which contrasts with the two-step process found for AlCoCrFeNi and involving successively the Al-Fe and Al-Co axes. Nevertheless, in both systems, PS initiates within the LRO domain, and except at lower temperatures, it remains surrounded by LRO boundaries, which suggests that an initially single-phased LRO alloy should separate into two or several LRO phases. Moreover, the PS process has a limited effect on the A2 part of the AlCrFeMnNi phase diagram, as it mainly entails a shrinking of the A2 band along the Cr-Fe axis. While this feature is common to both systems investigated hitherto, the situation is somewhat more complex for AlCrFeMnNi, since the shrinking becomes dissymmetrical below 1200 K and enhanced near the Cr corner of the AlCrFe section (compare 1300 and 1200 K on Fig. 6). This indicates that, compared to AlCoCrFeNi, the A2 part of the AlCrFeMnNi phase diagram is more significantly affected by the PS process, which below 1200 K involves LRO and A2 boundaries, whereas in AlCoCrFeNi the PS domain should mostly remain bounded by LRO phases down to 800 K. The description of such intricate trends, which can hardly be inferred from the present analysis, would benefit from more thorough investigations of the underlying conode structures.

Focusing on equiatomic AlCrFeMnNi, the CVM trends of this reference case are reported in Table 2, together with earlier values from PMF and MC. The agreement with MC simulations confirms the reliability of the CVM approach for the ordering temperature, while the latter was

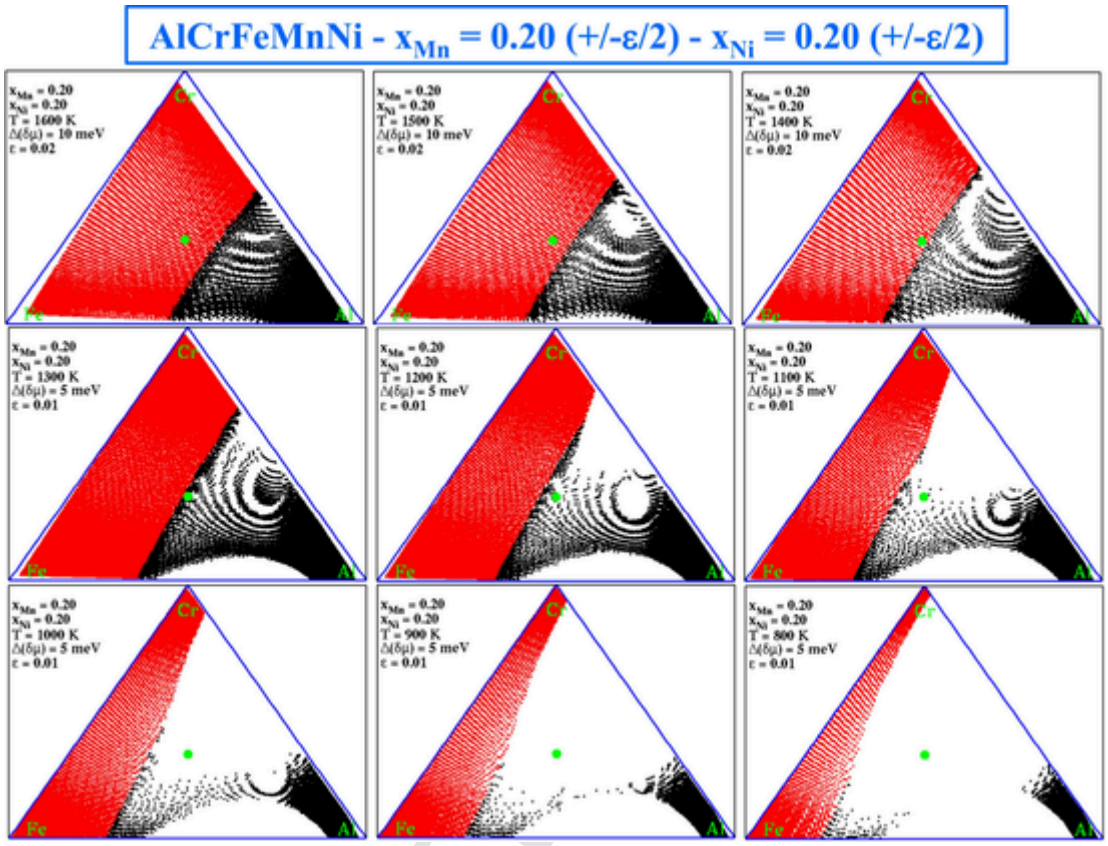

Fig. 6. Calculated phase diagram (CVM, irregular tetrahedron approximation) of bcc AlCrFeMnNi: isothermal pseudo-ternary sections in the AlCrFe plane for $x_{Mn} = x_{Ni} = 1/5$ including the equiatomic alloy (green spot). The disordered (A2) and ordered (B2-type) domains are displayed in red and black respectively. The simulation parameters ε and Δ(δμ) have the same meaning as previously (Fig. 5).

overestimated in PMF. As already noted for AlCoCrFeNi, interpreting the PS trends appears to be trickier, due to the difficulty to identify properly this phenomenon in MC simulations. The agreement on T_{PS} is however satisfactory between the CVM prediction and the upper value of the MC temperature range proposed previously [11]. As regards sublattice occupancies in the equiatomic alloy, Table 2 indicates that they can be written as $[Al > (Cr,Fe,Mn) > Ni]_{\alpha\beta}[Ni > (Cr,Fe,Mn) > Al]_{\gamma\delta}$ with a nearly random behaviour of Cr, Fe and Mn. The CVM equiatomic compound is thus $[Al\{CrFeMn\}]_{\alpha\beta}[Ni\{CrFeMn\}]_{\gamma\delta}$, which is identical to the earlier MC predictions, while the agreement with PMF is also correct. The energy parameters $\{H^{ij}\}$ relevant for AlCrFeMnNi can be classified as $H^{AlNi} < H^{AlFe} < H^{AlMn} < H^{AlCr} < H^{MnNi} \approx H^{CrMn} < H^{FeNi} < H^{CrNi} < H^{CrFe} < 0 < H^{FeMn}$. As expected, the lowest negative value H^{AlNi} is responsible for the strong partitioning between Al and Ni on the sublattices, but other features of the compound formula can hardly be inferred from this series of energy coefficients.

3.1.2. AlCrFeMnMo

The last system considered in this CVM work on MPEAs is AlCrFeMnMo, deduced from AlCrFeMnNi by Ni → Mo substitution, and which has recently formed the subject of experimental investigations [14]. In these experiments, the effect of a moderate composition change was also investigated, by comparing the equiatomic alloy and another alloy with composition $Al_{22}Cr_{22}Fe_{29}Mn_{20}Mo_7$, optimized by means of heuristic criteria for HEA selection. Surprisingly, in these earlier investigations, the analysis of the phases formed in AlCrFeMnMo during the heat treatments revealed the coexistence of two distinct disordered A2 solid solutions, whereas the PS process was expected to involve some LRO compound. Our previous attempt, by PMF modelling [13], to understand this surprising PS feature of AlCrFeMnMo, proved to be unsuccessful, since for both cases (equiatomic and optimized), PS was predicted to occur within the LRO domain. In addition, this PS feature also seems to conflict with the aforementioned CVM trends described in both AlCoCrFeNi and AlCrFeMnNi systems, namely PS preferentially occurring from a LRO initial state and inducing the formation of LRO phases. This context makes a CVM study of AlCrFeMnMo especially appealing, and for consistence with these earlier works, we follow a two-step canvas for description, associated to two distinct pseudo-ternary sections, which allows investigating in turn the equiatomic and optimized alloys.

Fig. 7 displays the isothermal pseudo-ternary sections in the AlFeMn plane, with constraints $x_{Cr} = x_{Mo} = 1/5$ including the equiatomic case, of the AlCrFeMnMo phase diagram for decreasing temperatures between 1300 and 800 K. The relevant temperature range is narrower than for AlCoCrFeNi and AlCrFeMnNi, the AlCrFeMnMo system being fully A2 disordered above 1400 K. As regards trend (i), LRO propagates from the Fe corner of the section, while the Al-Mn edge remains largely disordered, down to the lowest temperature considered (800 K), for which LRO reaches suddenly the Al-Mn axis around an Al:Mn ratio equal to 3:1. At this lowest temperature, a tiny LRO domain is surprisingly found to re-emerge near the Fe-Mn axis, which could not be clearly identified as a physically sensible feature or a numerical artifact. As for trend (ii), PS occurs near the Fe-Mn axis within the LRO domain, and has only limited effect on the A2 domain, except for a global shrinking of this domain. Focusing on the equiatomic alloy (green spot on Fig. 7), its LRO and PS temperatures from CVM are 1200 and 1000 K, which from Table 2 show good agreement with the earlier MC estimations (here again, for PS the upper bound of the MC range should be preferred). Also from Table 2, the sublattice occupancies for the B2-type compound are $[(Al,Mo) > (Cr,Mn) > Fe]_{\alpha\beta}[Fe > (Cr,Mn) > (Al,Mo)]_{\gamma\delta}$. The CVM compound formula derived from CVM, i.e. $[AlMo\{CrMn\}]_{\alpha\beta}[Fe\{CrMn\}]_{\gamma\delta}$,

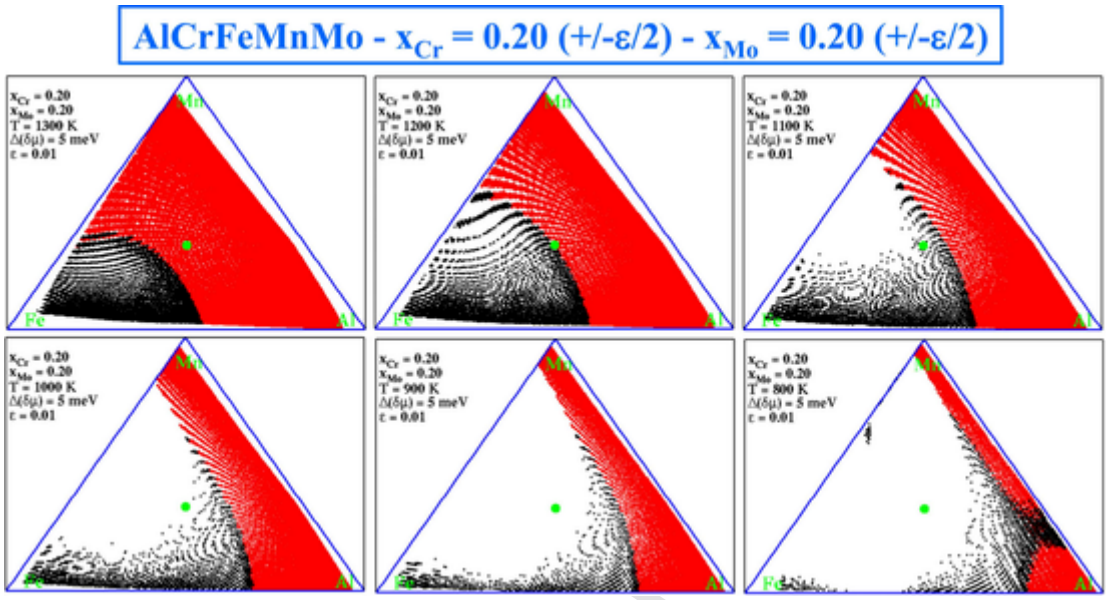

Fig. 7. Calculated phase diagram (CVM, irregular tetrahedron approximation) of bcc AlCrFeMnMo: isothermal pseudo-ternary sections in the AlFeMn plane for $x_{Cr} = x_{Mo} = 1/5$ including the equiatomic alloy (green spot). The disordered (A2) and ordered (B2-type) domains are displayed in red and black respectively. The simulation parameters ε and Δ(δμ) have the same meaning as previously (Fig. 5). The system is completely disordered (A2) for temperatures above 1300 K.

is thus in reasonable agreement with its MC and PMF counterparts. The energy parameters $\{H^{ij}\}$ relevant for AlCrFeMnMo being $H^{FeMo} < H^{AlFe} < H^{AlMn} < H^{AlMo} < H^{AlCr} \approx H^{MnMo} < H^{CrMn} < H^{CrFe} < 0 < H^{FeMn} < H^{CrMo}$, the major B2-type partitioning of (Al,Mo) and Fe on the sublattices can be related to the low negative values of H^{FeMo} and H^{AlFe}.

As a final case, we then consider pseudo-ternary sections (Fig. 8) of AlCrFeMnMo with constraints x_{Cr} = 22 % and x_{Mo} = 7 %, namely including the "optimized" alloy (green dot on Fig. 8). For the latter case, the LRO and PS temperatures from CVM (last row of Table 2) show good agreement with MC reference values, strengthening our above conclusions on CVM as a good compromise between computational cost and predictive accuracy. Compared to the previous case encompassing the equiatomic alloy (Fig. 7), the change of composition constraints ($x_{Cr} = x_{Mo} = 1/5 \rightarrow x_{Cr}$ = 22 % and x_{Mo} = 7 %), though relatively moderate, modifies significantly the global structure of the isothermal sections, probably in reason of the lower amount of Mo. Firstly, LRO is now found to propagate from the middle of the Al-Fe axis instead of the Fe corner, and at given temperature, the trend to disorder seems more pronounced than in the previous case (compare with Fig. 7). Noticeably, the composition change is also found to drastically alter the PS behaviour: a PS domain, initiating near the A2/B2 interface, suddenly penetrates into the A2 zone, and this quick propagation requires only a narrow range of temperature below 1000 K. This PS domain is consistent with the previously recalled observations of two distinct A2 phases obtained in experiments on AlCrFeMnMo [14]. In particular, the CVM suggests that the experimental "optimized" alloy may lie within the PS

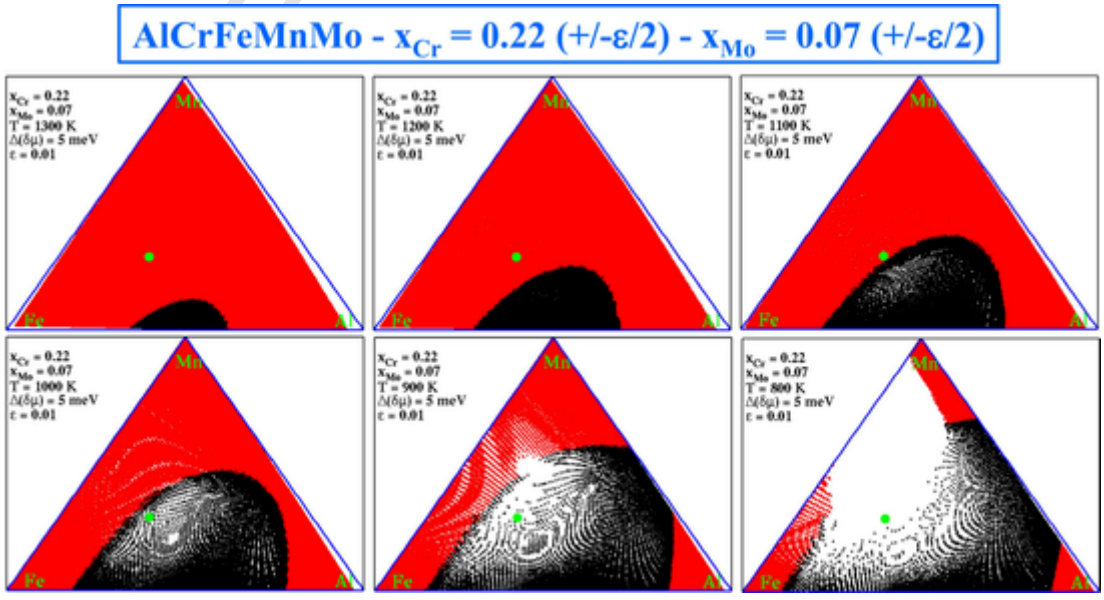

Fig. 8. Calculated phase diagram (CVM, irregular tetrahedron approximation) of bcc AlCrFeMnMo: isothermal pseudo-ternary sections in the AlFeMn plane for x_{Cr} = 22 % and x_{Mo} = 7 %. The green spot denotes the "optimized" alloy $Al_{22}Cr_{22}Fe_{29}Mn_{20}Mo_7$ investigated in previous experiments [14]. The disordered (A2) and ordered (B2-type) domains are displayed in red and black respectively. The simulation parameters ε and Δ(δμ) have the same meaning as previously (Fig. 5). The system is completely disordered (A2) for temperatures above 1300 K.

domain below 1000 K, and depending on more detailed features of the PS process, it may possibly give rise to new A2 phases, which thus may allow interpreting these counterintuitive experimental observations [14]. Here again, it should be emphasized that further inspection of PS, especially its associated structure of conodes, would be useful to confirm these trends. Nevertheless, our results clearly confirm the interest of CVM calculations in the context of MPEAs, especially when unexpected PS processes are to be dealt with in experiments.

4. Discussion

In this work, we have tried to characterize the ability of the CVM approach to investigate the thermodynamic properties of MPEAs. From a practical point of view, the CVM is found to represent a good compromise between computational efforts and accuracy to reach this goal, especially when the general important MPEA trends to ordering and phase separation are at stake. Noticeably, the CVM procedure illustrated above allows drawing isothermal pseudo-ternary sections of MPEA phase diagrams, on which these trends can easily be identified. Moreover, due to the frequent cubic structure of MPEAs, the CVM formulation in the tetrahedron approximation is well suited for these systems. In the present state of our work, the most significant limitation of the CVM is due to our choice to stay in a fully grand-canonical framework, implying to explore a composition domain somewhat larger than the desired pseudo-ternary section, whereas the earlier "composition-constrained" formulation of PMF was designed to reach immediately this section [13]. In future works, it may thus be fruitful to investigate more thoroughly whether some similar "composition-constrained" CVM approaches could be designed and implemented. This interesting task is however not mandatory, since the CVM approach described above seems to offer sufficient efficiency.

It is instructive to confront the current CVM phase diagrams of MPEAs to their counterparts derived previously from PMF [13]. In AlCoCrFeNi, the isothermal sections from CVM at 1600 K and from PMF at 2000 K are found to be almost identical. Such a correspondence can also be observed in AlCrFeMnNi and AlCrFeMnMo, the PMF and CVM pseudo-ternary sections explored being almost similar at a same temperature, ~1600 K and ~1300 K, respectively. This suggests that PMF may be used with success for MPEAs in the higher temperature range, i.e. as long as the alloy is single-phased, in order to sketch the phase diagram and easily localize the A2 and LRO domains. Nevertheless, this analogy between PMF and CVM remains limited, since the emergence of PS at cooling is a much earlier phenomenon in CVM than in PMF, which severely restricts the temperature domain of validity of PMF. Therefore, while for higher temperatures a PMF phase diagram may be viewed as an approximate distorted picture of a more realistic CVM one drawn at a temperature lower by a few hundred K, the major drawback of PMF for practical applications lies in the difficulty to infer the lowest temperature for which this correspondence remains valid. This emphasizes the necessity, in MPEA studies, of supplementing the PMF approach with more reliable CVM calculations, at least for selected compositions and temperatures.

While this work was mainly devoted to overall long-range ordering and phase separation trends in MPEAs, the CVM may also conveniently yield more detailed information related to short-range ordering, via the analysis of the correlation functions of the relevant clusters (here tetrahedron, triplets, 1N and 2 N pairs). This may help elucidate the role of the frequently used pair energetics in the thermodynamic behaviour of MPEAs. More specifically, with the energetics considered above and restricted to 1N pairs, it might be instructive to investigate the consequences of this very low range of energetic interactions on the chemical correlations (short-range ordering) beyond the first neighbour shell. Such an analysis should however be made quite cumbersome by the relatively high number of correlation functions, and was thus left for future. In addition, considering the simplicity and importance of pair models for MPEA configuration energies, obtaining experimental information on these delicate issues, e.g. from high-resolution atomic-scale techniques such as EXAFS or XANES, would be useful to estimate the validity of these models, and may suggest ways to improve them. Moreover, another valuable feature of the CVM, allowing complementary studies, concerns its ability to provide accurate and handsome explicit expressions for MPEA entropies [19,20]. In the context of HEAs, often reputed to have remarkable properties related to high configurational entropies, the CVM makes it possible to evaluate quantitatively the deviations of MPEA entropies from the ideal case (kLog(5) for quinaries), and thus to get a deeper insight into the "high entropy" assumption and its practical consequences for MPEAs.

A significant result pointed out by our CVM calculations was obtained for the AlCrFeMnMo system, in which moderate composition changes were found to entail strong effects on LRO and PS trends (compare Figs. 7 and 8), in good agreement with experiments. In this respect, while this is difficult to appreciate fully from the partial views given by several pseudo-ternary sections, AlCrFeMnMo may behave somewhat differently from AlCoCrFeNi and AlCrFeMnNi. It would be highly useful to establish firm connections between these changes of trends among neighbouring MPEA systems and the underlying alloy energetics, but even in the case of the very simple 1N pair models selected, this appears to be a hard task. In this difficult context, it is worth recalling here the evolution of the model alloy energetics [9] when shifting from AlCrFeMnNi to AlCrFeMnMo (see Fig. 4 of Ref. [13]). Namely, while the moderately attractive interactions of Mn with either Ni or Mo are roughly equal, this evolution is apparently due to the sensitive interactions between Ni or Mo and (Al;Fe). To state it simply, Al and Fe roughly exchange their roles when associated with Ni or Mo: the strongly attractive Al-Ni interaction (resp. moderately attractive Fe-Ni) turns into a moderately attractive Al-Mo (resp. strongly attractive Fe-Mo) one. The picture is however made more intricate by a second noticeable feature, namely the change of the weak attractive Cr-Ni interaction into a weakly repulsive Cr-Mo one, and the connections with the respective LRO and PS trends of AlCrFeMnNi and AlCrFeMnMo remain to be further clarified.

As for most systems, the central issue to achieve reliable MPEA thermodynamics from atomic-scale simulations is the validity of the configurational energy model. Whereas the CVM can a priori handle any such model, its handsome "tetrahedron" formulation requires short-ranged pair interactions, limited in the bcc case to second-nearest neighbours. In this study, our main concern was to get an overall knowledge of the merits of the CVM for MPEAs, and we therefore made use of a simple alloy energetics limited to first-nearest neighbour pairs, with ab initio-based interaction energy coefficients taken from a previous work [9]. In future studies, a valuable issue, possibly involving CVM simulations in close conjunction with dedicated experiments, may concern more precise analyses of the relevance of such energetics for MPEAs. It is an immediate task to include second-nearest neighbour pairs in the energetics and CVM thermodynamics of bcc MPEAs. This would help determine whether such refinements of MPEA energy models are only of moderate influence (e.g. on the emergence of other types of B2-related LRO), or may more drastically modify the main phase diagram structure as concerns disordered/LRO and PS domains. However, the critical issue here lies in the choice of these additional 2 N pair interactions, since taking the latter into account may imply to revisit the values of the 1N coefficients already selected [9]. This is a very intricate issue, since the approximations that should be examined are twofold, i.e. the pair character of the interactions and their range, and each aspect may deserve separate investigations. In this context, it may be valuable to resort to "direct" ab initio approaches providing various interaction parameters, either pairs or not and with tunable ranges. For instance, such direct approaches have been employed recently [12] to study equiatomic alloys in the CoCrFeMnNi system. Within a framework limited to pair interactions, this recent work enlightened the possibility

that, depending on the alloy considered, ranges beyond 2 N pairs may be required, hence some need for further improvements of the present CVM approach. Another difficulty may be due to the fact that the chemical interactions derived from such direct methods inherently depend on the alloy composition. This somewhat restricts the applicability of the CVM and PMF frameworks to get an overall picture of MPEA phase diagrams, and a compromise may consist in using such interactions, frequently referred to the equiatomic MPEA of a given system, to explore a limited part of the phase diagram around the equiatomic composition (e.g. as shown on Fig. 4, using the reduced parameter α). On the whole, gathering these various possibilities of refinements for ab initio-based MPEA energetics and CVM-based MPEA thermodynamics provides an encouraging picture for future MPEA studies, with reasonable hope to turn atomic-scale simulations into a useful guide for alloy selection, especially if these simulations are coupled with experiments.

The present CVM study suggests that PS trends in MPEAs may be especially difficult to describe with accuracy. In order to illustrate this point for the case of AlCoCrFeNi (Fig. 5), it may be noticed that, while the primary PS domain observed along the Al-Fe axis is widely spread at 900 K, a secondary PS domain is also found to open at this temperature along the Al-Co axis. Since this occurs at a cooling stage for which PS reaches the equiatomic composition, the simultaneous presence of two PS domains increases the intricacy of characterizing the multi-phase material that should result from the PS process of the equiatomic alloy. This emphasizes the complexity of PS phenomena in MPEAs as regards the numbers, ordering states and compositions of the phases in equilibrium. To help elucidate these issues, a more thorough analysis, including careful inspection of the conode structures generated by chemical potential scan, may be helpful. However, such a task should not be straightforward, due to the non-planar character of conodes, implying that the equilibrium phases occurring at PS are usually not located within a single isothermal section, and this intricate task was thus left for future works. Finally, to complete our current remarks on PS trends of MPEAs, it should be noted that, contrary to MC [11] and PMF [13], no critical ambiguity arises in CVM for the identification of PS domains, which is a clear advantage of CVM over both other approaches.

As mentioned in the introduction, CALPHAD-type phenomenological approaches provide powerful tools to explore alloy thermodynamics. While most such studies have been concerned hitherto with various alloys built on a single base element (steels, Al alloys…), recent works [21–23] have demonstrated that such calculations, either relying on databases for traditional alloys or on newly developed databases, can also be used for MPEAs with reasonable accuracy. In this context, atomic-scale investigations of MPEA thermodynamics, such as those described in the present work, can be viewed as complementary tools, offering many possibilities to refine CALPHAD-type databases, especially in composition domains for which input data are difficult to extract from experiments. While the success of incorporating atomic-scale thermodynamic insights into phenomenological databases is widely dependent on the robustness of the atomistic energy model, this requirement should be increasingly fulfilled [12] by resorting to first-principles methods (as discussed above in this section), since the latter offer firmly established routes to determine reliable energy coefficients, especially pair interactions.

5. Conclusion

This work was devoted to the presentation of an original Cluster Variation Method (CVM) procedure designed to perform efficient explorations of large composition spaces characterizing multi-principal-element alloys (MPEAs), by means of pseudo-ternary isothermal sections of MPEA phase diagrams. The proposed approach may conveniently help gain better insight into two essential features of MPEAs, namely long-range ordering (LRO) and phase separation (PS), both being of special practical importance for this wide class of materials. Its efficiency was demonstrated by successive applications to several quinary bcc-based MPEAs within {Al,Co,Cr,Fe,Mn,Mo,Ni}. For all MPEAs explored, the reliability of characteristic LRO and PS temperatures deduced from CVM was confirmed by comparison with exact, but computationally much more expensive, Monte-Carlo (MC) simulations. Compared to other approaches such as MC and point-mean-field, the CVM is efficient to characterize without unambiguity the formation of PS domains in MPEAs. Noticeably, in the case of AlCrFeMnMo, our CVM simulations provide elements to interpret unexpected trends observed in earlier experiments on these MPEAs. The proposed approach also lends itself to various future applications, since it can be (i) extended towards many other MPEAs, (ii) adapted to other MPEA energetics, including possibly more realistic composition-dependent interactions, e.g. those derived from accurate ab initio methods such as the Coherent Potential Approximation, and (iii) used in conjunction with reference experiments carried out to estimate the relevance of atomic-scale energy models of MPEAs. All these elements give reasonable confidence that atomic-scale simulations may gain enhanced utility as a guide for MPEA selection.

CRediT authorship contribution statement

Rémy Besson: Analytic modelling, Computer simulations, Manuscript writing.

Declaration of Competing Interest

The authors declare that they have no known competing financial interests or personal relationships that could have appeared to influence the work reported in this paper.

Data Availability

No data was used for the research described in the article.

Acknowledgments

The author thanks the Centre de Ressources Informatiques (C.R.I.) of the Université de Lille for computational facilities.

Appendix

Average configurational energy expression of bcc alloys for irregular tetrahedron approximation of CVM.

If only 1N pairs are considered, the connection between the J and ε coefficients reads, for bcc ternary A-B-C alloys (with straightforward extension to quinary cases, δ = Kronecker symbol):

$$\begin{aligned}6\varepsilon_{ijkl} = {} & J_{1N}^{BB}\left[\delta_{i1}\delta_{k1}+\delta_{i1}\delta_{l1}+\delta_{j1}\delta_{k1}+\delta_{j1}\delta_{l1}\right] \\ & + J_{1N}^{CC}\left[\delta_{i2}\delta_{k2}+\delta_{i2}\delta_{l2}+\delta_{j2}\delta_{k2}+\delta_{j2}\delta_{l2}\right] \\ & + J_{1N}^{BC}\left[\left(\delta_{i1}\delta_{k2}+\delta_{i2}\delta_{k1}\right)+\left(\delta_{i1}\delta_{l2}+\delta_{i2}\delta_{l1}\right)\right. \\ & \left. + \left(\delta_{j1}\delta_{k2}+\delta_{j2}\delta_{k1}\right)+\left(\delta_{j1}\delta_{l2}+\delta_{j2}\delta_{l1}\right)\right]\end{aligned}$$

References

[1] M.C. Gao, J.-W. Yeh, P.K. Liaw, Y. Zhang, in: High-Entropy Alloys - Fundamentals and Applications, Springer, 2016.
[2] D.B. Miracle, O.N. Senkov, A critical review of high entropy alloys and related concepts, Acta Mater. 122 (2017) 448–511.
[3] T.S. Srivatsan, M. Gupta, in: High Entropy Alloys - Innovations, Advances and Applications, CRC Press, 2020.
[4] R. Besson, Understanding phase equilibria in high-entropy alloys: II. Atomic-scale study of incorporation of metallic elements in Cr carbides – application to equilibrium with AlCrFeMnMo, J. Alloy. Compd. 874 (2021) 159959.
[5] F. Ducastelle, Order and Phase Stability in Alloys, North-Holland, 1991.
[6] A. Fernández-Caballero, M. Fedorov, J.S. Wróbel, P.M. Mummery, D. Nguyen-Manh, Configurational entropy in multicomponent alloys: matrix formulation from

ab Initio based Hamiltonian and application to the FCC Cr-Fe-Mn-Ni system, Entropy 21 (2019) 68.
[7] D. Sobieraj, J.S. Wróbel, T. Rygier, K.J. Kurzydłowski, O. El Atwani, A. Devaraj, E. Martinez, D. Nguyen-Manh, Chemical short-range order in derivative Cr–Ta–Ti–V–W high entropy alloys from the first-principles thermodynamic study, Phys. Chem. Chem. Phys. 22 (2020) 23929.
[8] Y. Ikeda, B. Grabowski, F. Körmann, Ab initio phase stabilities and mechanical properties of multicomponent alloys: a comprehensive review for high entropy alloys and compositionally complex alloys, Mater. Charact. 147 (2019) 464–511.
[9] M.C. Troparevsky, J.R. Morris, P.R.C. Kent, A.R. Lupini, G.M. Stocks, Criteria for predicting the formation of single-phase high-entropy alloys, Phys. Rev. X 5 (2015) 011041.
[10] L.J. Santodonato, P.K. Liaw, R.R. Unocic, H. Bei, J.R. Moris, Predictive multiphase evolution in Al-containing high-entropy alloys, Nat. Commun. 9 (2018) 4520.
[11] W. Sekkal, R. Besson, A. Legris, Atomic-scale modeling of structural phase transformations in AlCrFeMnMo high-entropy alloys during thermal treatments, J. Alloy. Compd. 876 (2021) 160201.
[12] C.D. Woodgate, J.B. Staunton, Compositional phase stability in medium-entropy and high-entropy Cantor-Wu alloys from ab initio electron Landau-type theory and atomistic modeling, Phys. Rev. B 105 (2022) 115124.
[13] R. Besson, Ordering and phase separation in multi-principal-element metallic alloys: Contribution from mean-field atomic-scale modelling and simulation, J. Alloy. Compd. 898 (2022) 162842.
[14] T. Stasiak, S.N. Kumaran, M. Touzin, F. Beclin, C. Cordier, Novel multicomponent powders from the AlCrFeMnMo family synthesized by mechanical alloying, Adv. Eng. Mater. 21 (2019) 1900808.
[15] R. Besson, J. Dequeker, L. Thuinet, A. Legris, Ab initio thermodynamics of complex alloys: the case of Al- and Mn-doped ferritic steels, Acta Mater. 169 (2019) 284–300.
[16] P.E.A. Turchi, A. Gonis, The Cluster Variation Method and Some Applications, A. Finel, in statics and dynamics of alloy Phase Transformations, Plenum Press, New York, 1994.
[17] H. Ackermann, G. Inden, R. Kikuchi, Tetrahedron approximation of the cluster variation method for b.c.c. alloys, Acta Metall. 37 (1989) 1–7.
[18] C. Colinet, G. Inden, R. Kikuchi, CVM calculation of the phase diagram of b.c.c. Fe-Co-Al, Acta Metall. Mater. 41 (1993) 1109–1118.
[19] C.G. Schön, T. Duong, Y. Wang, R. Arroyave, Probing the entropy hypothesis in highly concentrated alloys, Acta Mater. 148 (2018) 263–279.
[20] C.G. Schön, T. Duong, Y. Wang, R. Arroyave, A proof of concept: thermodynamics of aluminum - transition metal highly concentrated alloys, J. Alloy. Compd. 781 (2019) 595–605.
[21] F. He, Z. Wang, P. Cheng, Q. Wang, J. Li, Y. Dang, J. Wang, C.T. Liu, Designing eutectic high entropy alloys of $CoCrFeNiNb_x$, J. Alloy. Compd. 656 (2016) 284–289.
[22] F. He, Z. Wang, B. Han, Q. Wu, D. Chen, J. Li, J. Wang, C.T. Liu, J.-J. Kai, Solid solubility, precipitates, and stacking fault energy of micro-alloyed CoCrFeNi high entropy alloys, J. Alloy. Compd. 769 (2018) 490–502.
[23] F. He, D. Chen, B. Han, Q. Wu, Z. Wang, S. Wei, D. Wei, J. Wang, C.T. Liu, J.-J. Kai, Design of $D0_{22}$ superlattice with superior strengthening effect in high entropy alloys, Acta Mater. 167 (2019) 275–286.